

NAVY RESEARCH SECTION  
SCIENCE DIVISION  
REFERENCE DEPARTMENT  
LIBRARY OF CONGRESS

DECLASSIFIED

AECD - 2705

APR 4 1950

APR 1 1950

UNITED STATES ATOMIC ENERGY COMMISSION

NUCLEAR CROSS SECTIONS FOR 95-MEV NEUTRONS

by

James DeJuren  
Norman Knable

University of California  
Radiation Laboratory

This document is reproduced as a project report and  
is without editorial preparation. The manuscript has  
been submitted to The Physical Review for possible  
publication.

**DISTRIBUTION STATEMENT**

Approved for public release  
Distribution Unlimited

Date of Manuscript: June 10, 1949  
Date Declassified: September 15, 1949

Issuance of this document does not constitute  
authority for declassification of classified  
copies of the same or similar content and title  
and by the same authors.

Technical Information Division, ORE, Oak Ridge, Tennessee  
AEC, Oak Ridge, Tenn., 3-10-50--850-A14035

PRINTED IN USA  
PRICE 10 CENTS

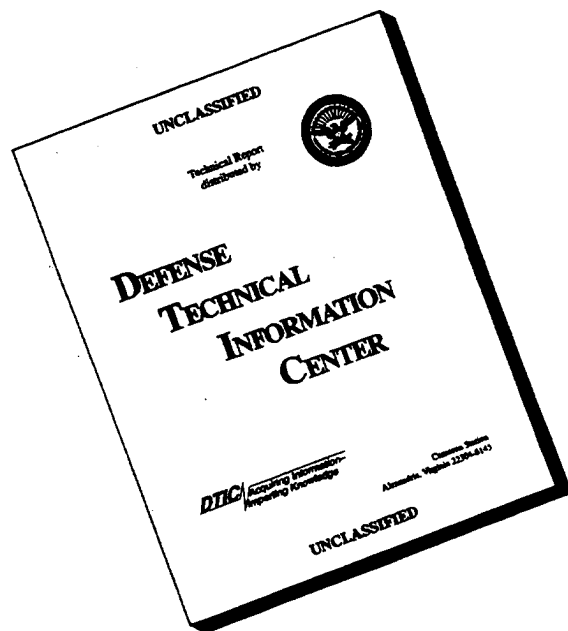
DECLASSIFIED

DTIC QUALITY INSPECTED 3

19960920 067

U-9833

# DISCLAIMER NOTICE



**THIS DOCUMENT IS BEST QUALITY AVAILABLE. THE COPY FURNISHED TO DTIC CONTAINED A SIGNIFICANT NUMBER OF PAGES WHICH DO NOT REPRODUCE LEGIBLY.**

## NUCLEAR CROSS SECTIONS FOR 95-MEV NEUTRONS

By James DeJuren and Norman Knable

### ABSTRACT

The total cross sections of twelve different elements were measured using the neutron beam from the 184-in. cyclotron, operating with deuterons. Bismuth-fission ionization chambers were employed as both monitor and detector in conventional "good geometry" attenuation measurements in the neutron flux emerging from the 3-in.-diameter collimating port in the 10-ft-thick concrete shielding. The mean energy of detection of the neutrons in this experiment is estimated to be 95 Mev.

Measurements were also made with a monitor and detector placed inside the concrete shielding where an intense neutron flux over a large area could be obtained. Attenuators of four different elements were placed in front of the detector in a "poor geometry" arrangement so that attenuation was due essentially to inelastic collisions which degrade the neutron energy below the fission threshold. A second detector was placed outside the concrete shielding in the collimated neutron beam in line with the neutron source, absorber, and first detector. Attenuation in it is caused by both inelastic and elastic scattering. By this arrangement the ratio of inelastic to total cross section can be determined directly in one experiment.

The nuclear radii as calculated from the observed cross section, using the theory of the transparent nucleus, vary as  $1.38 \times 10^{-13} A^{1/3}$  cm. In this energy range the ratios of the inelastic to total cross sections are all less than one-half.

### INTRODUCTION

Several experiments have been conducted to measure the cross sections of nuclei with neutrons. They have been spaced at intervals corresponding to the periods when an increase in the energy of the bombarding neutrons was made available. It was thought that as the available energies increased, the measured cross sections would tend to become independent of the energy of the bombarding particle. The results of these previous measurements are summarized in a recent paper of Cook, McMillan, Peterson, and Sewell,<sup>1</sup> which describes a measurement of cross sections using the neutrons produced by 190-Mev deuterons of the 184-in. cyclotron.

The threshold energy of the reaction used for detecting the neutrons  $C^{12}(n,2n)C^{11}$  is 20 Mev, and an average cross section is obtained for neutrons having the average energy of the distribution produced in the cyclotron, modified by the  $(n,2n)$  cross-section energy dependence. This work showed the expected  $A^{1/3}$  variation of the nuclear radius, calculated from an opaque nuclear model, for heavy nuclei but clearly indicated that the light nuclei (carbon and lighter) had smaller apparent radii than would be expected from an  $A^{1/3}$  law. This effect was attributed to the transparency of the light nuclei for neutrons of short wavelengths.

These results indicated the need for a similar experiment to be done at higher energies, in order to investigate the energy dependence of the effect. The estimated average energy of detection in the early experiment was 83 Mev. In the experiment to be described below, the same source of neutrons

was employed, but a bismuth-fission ionization chamber<sup>2</sup> with a threshold of about 50 Mev and a mean detection energy of 95 Mev served as the detector. In addition to raising the average detection energy this high threshold served a second purpose; it allowed measurement of the cross sections for inelastic processes.

Such a measurement was necessary, for one could no longer assume that the cross sections for inelastic scattering and for elastic scattering were equal to each other and to one-half the total cross sections, as would be expected from an opaque model of the nucleus. The nuclear transparency would cause the ratio of inelastic and elastic scattering cross sections to be energy dependent.

Fernbach, Serber, and Taylor<sup>3</sup> have, by assuming a model of the nucleus which has an absorption coefficient and an index of refraction, arrived at a formula for the radius of the nucleus in terms of the total cross section which for the experimental cross sections given below shows the radii of the nuclei to be directly proportional to  $A^{1/3}$  within the limits of experimental error. The same good fit has been made with the data of the previous experiment, using the index of refraction and absorption coefficient corresponding to the neutron momentum of the average energy of detection in that experiment.

The total cross sections of twelve different nuclei were measured, employing bismuth-fission ionization chambers as both monitor and detector in conventional "good geometry" attenuation measurements in the neutron flux emerging from a 3-in.-diameter collimating port in the 10-ft-thick concrete shielding.

Measurements were also made with a monitor and detector placed inside the concrete shielding where an intense neutron flux over a large area could be obtained. Attenuators of four different elements were placed in front of the detector, so that the angle subtended by the attenuator was greater than the angle at which the differential scattering cross section of the attenuator nuclei fell to 1 per cent of its value in the forward direction. This arrangement simulated the situation in which a plane wave of neutrons strikes a slab of material infinite in area, so that attenuation is due solely to inelastic collisions. Measurements with higher threshold detectors gave results that agreed within the probable errors, thus confirming our assumption that an inelastic collision reduces the neutron energy below the threshold for bismuth fission.

A second detector was placed outside the concrete shielding in the collimated beam in line with the neutron source, attenuator, and first detector. Attenuation of the beam for the last detector is caused by both elastic and inelastic scattering. By this arrangement the ratio of inelastic to total cross sections can be measured directly in one experiment.

## COUNTERS AND NEUTRON DETECTION

**Counters.** The ionization chambers<sup>2</sup> employed outside the concrete shielding contained 31 aluminum discs 1/32 in. thick and 2 in. in diameter (Fig. 1). Alternate disks were coated with thin layers of bismuth, and the separation between adjacent disks was 3/8 in. The disks of the chambers used as monitors were plated with bismuth 1.0 to 1.5 mg/cm<sup>2</sup> thick; the detector disks were plated with bismuth 10 mg/cm<sup>2</sup> thick. For exposure to equal neutron flux the detector counting rate is three to four times that of the monitors. The chambers employed in the "poor geometry" measurements inside the shielding were of a shallow design, containing three plates 4.5 in. in diameter, 3/4 in. apart. Thin bismuth layers were used (as in the monitors described above). The fragments produced in fission of bismuth by the high-energy neutrons experience their greatest rate of energy loss at the beginning of their ranges, since they are initially multiply ionized and recombine with electrons as their velocities decrease. Hence most of the ionization in the argon gas occurs near the negative, bismuth-coated plates. The electrons formed are collected on the aluminum plates (field strength 500 v/cm), and the resulting pulses are amplified by means of linear amplifiers.

**Pulse Characteristics.** The number of ions produced by a bismuth fission fragment is much greater than that produced by an alpha particle or proton given off by a spallation reaction in the chamber. Consequently it will take coincidences of several spallation reactions to give a pulse as large as a fission pulse. The gas used in the chambers was argon with 3 per cent carbon dioxide, and

the pressure was adjusted so that the range of the fission fragments was approximately equal to the separation of the plates, since at a higher pressure the total ionization in the gas from a fission fragment would be unchanged, but the ionization from an alpha particle would increase proportionally with pressure. If at a given neutron intensity the logarithm of the counting rate is plotted against the discriminator voltage (Fig. 2), a curve with a broad plateau is obtained. The variation of the counting rate on the plateau is usually 1 to 2 per cent per volt change of discriminator voltage. If the logarithm of the ratio of the number of counts of the chamber to a fixed monitor is plotted against discriminator voltage, a similar curve results. If the neutron intensity is increased, the rapidly varying "pileup" region of the curve, owing to pulses from coincident spallation reactions, is shifted to the right, but the remainder of the curve is unchanged. This agrees with what would be expected from theoretical considerations, which show the number of "pileups" to be a much more rapidly increasing function of the neutron intensity than is the number of fissions. Variation of neutron intensity thus affords a criterion for distinguishing fission pulses from "pileups" of spallation products.

The stability of the amplification and discrimination voltages was periodically checked by feeding in fixed voltage pulses, and it was determined that the experimental errors so incurred were less than the statistical errors of counting.

#### EFFECTIVE NEUTRON DETECTION ENERGY

The neutron beam was produced by bombarding a 0.5-in. beryllium target with 190-Mev deuterons in the 184-in. cyclotron. The neutrons produced by "stripping" have an energy distribution theoretically predicted by Serber<sup>4,5</sup> and checked experimentally with proton-recoil counters<sup>6</sup> and by proton recoils in a cloud chamber.<sup>7</sup> The variation of the fission cross section with neutron energy was investigated by Wiegand and Kelly<sup>8</sup> by varying the radius of the target probe in the 184-in. cyclotron. As there is a spread in neutron energies for each radius, and the more energetic neutrons in each energy spectrum have the highest fission efficiency, the curve of bismuth-fission cross section as a function of neutron energy may be even steeper than indicated. If the fission efficiency and neutron distribution for corresponding energy intervals are multiplied, a curve results proportional to the detection efficiency as a function of neutron energy (Fig. 3). The curve is similar to the original neutron distribution; both curves have an energy spread of about 26 Mev at half maximum, but the average energy of the neutrons detected by fission is about 95 Mev.

#### EXPERIMENTAL ARRANGEMENTS

Arrangement for Total Cross Sections. The monitors and detectors employed in measuring total cross sections were aligned outside the concrete shielding by means of x-ray film (which was exposed to  $\gamma$  rays formed when deuterons struck the target). The attenuators were placed behind the monitor at a distance of 100 in. from the detector (Fig. 4), so that the detector subtended a solid angle of 0.0003 steradian at the attenuator. A steel collimator 18 in. long with a 1-in.  $\times$  1.5-in. cross-sectional aperture was employed in all but the first few experiments. The correction for small-angle scattering was negligible when the collimator was used, and the maximum correction without the collimator was only 2.2 per cent for the lead cross section.

Arrangement for Inelastic Cross Sections. The two shallow-type chambers mentioned earlier were equipped with cathode followers that would function in the stray magnetic field inside the concrete shielding. These chambers could be placed in the broad neutron beam<sup>5</sup> outside the cyclotron tank. One chamber was placed in the central portion of the beam in line with the probe and collimator (Fig. 4). Absorber slabs could be placed in front of this chamber in "poor geometry" fashion. The second chamber was placed to one side of the absorbers to serve as a monitor. The absorbers were stacked in a conical array, as shown in Fig. 4. The angular distribution of elastically scattered neutrons from nuclei is peaked in the forward direction, and even for carbon the fraction singly-scattered more than 45 deg is negligible, so the conical half angle of 45 deg employed permitted

essentially all the elastically scattered neutrons to enter the poor geometry detector, which would have entered even if the slabs were infinite in area. Therefore the attenuation is a measure of the cross section for inelastic collision. A detector was also placed outside the shielding, as previously mentioned, in line with the collimated beam, so measurements of total and inelastic cross sections could be measured simultaneously.

The total thickness of attenuators used was restricted by the condition that the flux should be uniform over the first disk (largest in area). A survey of the uniformity was made by moving a shallow fission chamber with 2-in.-diameter bismuth-coated plates over the region where the poor geometry attenuators were placed. The neutron flux was uniform (within 95 per cent of the peak value) over an area 7 in. in radius. Disks greater than 8 in. in radius could not be used because the cyclotron deflector housing reduced the beam intensity at that radius. The attenuation was exponential over more than two inelastic mean free paths of copper, with no transition effects.

Magnitude of Attenuation Employed. As the attenuation was exponential, within the probable errors, for both the "good" and "bad" geometry experiments, it was not necessary to measure the slope of a semi-log plot of the intensity versus thickness. Measurements were made with between one and two mean free paths of material.

For the experiments performed outside the shielding the monitor and detector counting rates were normally about equal with no attenuator present. The statistical error in the value of the cross section measured is equal to the statistical error of counting divided by the number of mean free paths of absorber. The principal counting error results from the detector reading with attenuator present. The most efficient length for a cross-section determination was slightly over two mean free paths of material, but to minimize diffraction scattering into the detector, usually a length of less than two mean free paths was employed.

## ATTENUATOR MATERIALS

Physical Properties. The metals used in the experiments were usually machined cylinders and were measured by two different observers with micrometer or vernier calipers and carefully weighed. The liquids employed were weighed in a 500-ml volumetric flask, which was first calibrated by weighing distilled water at 19.1°. The measured value of the density was 0.9980 g/ml, while the accepted value is 0.9984 g/ml.

The liquids were held in a 3 in. inner diameter cylindrical brass holder of variable length, with 1/16-in.-thick brass end caps. During an experiment several counting intervals were employed with the holder alternately filled and empty.

The nitrogen cross section was derived from melamine,  $C_3H_6N_6$ . The melamine was carefully tamped in the brass holder in an effort to make the density as uniform as possible. An alternate empty holder with similar caps was employed during the "blank" counting intervals.

When the holder was used, the beam from the 1-in.  $\times$  1.5-in. collimator was always carefully centered by means of x-ray film to minimize scattering from the brass walls.

Purity of Attenuators. Chemically pure materials were used, and the effect of minute impurities on the values obtained is negligible.

Because of its theoretical importance the total cross section of hydrogen was measured carefully on three separate occasions, using pentane-carbon differences. Six graphite cylinders were machined to fit in the brass liquid holder. The length of the holder was adjusted (43 in.) so that the mass per unit area of carbon in the graphite was equal to the carbon in the pentane employed. The graphite cylinders were distributed along the length of the holder to simulate the distribution of carbon in the pentane. A counting interval was first taken with graphite in the holder. When the pentane was substituted, the attenuation in the detector over the previous case was due solely to the hydrogen in the pentane. Hence the counting errors are due to these cycles only, and the hydrogen cross section is directly obtained without the need of blank cycles, which would introduce added statistical errors. As only 0.5 mean free path of hydrogen was present and the statistical error of the cross section is the counting error divided by the mean free path, it was important to use the counting time efficiently.

The graphite and pentane were analyzed by the Pacific Chemical Laboratories for impurities, which were as follows:

Sample	Impurities	Percentage
Graphite	Silicon	0.052 per cent
	Sulfur	0.067 per cent
	Iron	0.011 per cent
	Others	0.020 per cent
Pentane	Sulfur	0.045 per cent

The error introduced by these impurities is not significant.

The difference between the deuterium and hydrogen cross sections was determined directly in a similar experiment by filling the holder alternately with equal numbers of  $D_2O$  and  $H_2O$  molecules. The heavy water was 99.87 per cent  $D_2O$  by weight.

## RESULTS

Total Cross Sections. The data for the total cross sections measured outside the shielding are given in Table 1. Corrections for diffraction scattering are included in a few cases where this is significant. Statistical errors given are in terms of standard deviations. The effect of background was investigated by placing fourteen mean free paths of various absorbers between detector and monitor. Without absorbers 950 detector counts were obtained for 1,000 monitor counts. With absorbers no detector counts were obtained for 3,600 monitor counts. Even a few detector counts would have meant negligible error from background. As the chambers have excellent high-voltage and discriminator characteristics, the error introduced by the equipment is probably less than 1 per cent. Repeated measurements have given differences that appear to be purely statistical.

Inelastic Cross Sections. The inelastic cross-section measurements are subject to greater sources of error. The "poor geometry" detectors count inelastically scattered neutrons or neutrons ejected from nuclei if their energies are above the threshold for bismuth fission. Therefore the inelastic cross sections obtained represent a lower limit to the true values. However, it is not expected that the contribution of neutrons over threshold energy from inelastic processes is large enough to modify the present interpretations.

Elastically scattered neutrons will have a greater path length than undeviated neutrons in both the absorber and the bismuth layer of the detector. The relative probability of detection for different neutron paths is discussed in the appendix. Table 2 contains the experimental results. The ratio of  $\sigma_i/\sigma_t$  is given since it is independent of density determinations of the material used and is measured directly. The total cross sections listed in Table 2 were measured with "better" geometry than those in Table 1 and therefore require no corrections for diffraction. Actually dural was used, instead of aluminum, but the correction for the impurities (mainly copper) is negligible for the ratio of  $\sigma_i/\sigma_t$ .

An attempt was made to measure the ratio of  $\sigma_i/\sigma_t$  for carbon and copper, using gold fission for neutron detection, since gold presumably has a higher fission threshold than bismuth. The values obtained were

Element	$\frac{\sigma_i}{\sigma_t}$	$\sigma_t$
Carbon	$0.42 \pm .04$	$0.48 \pm .35$
Copper	$0.38 \pm .015$	$1.92 \pm .06$

The counting rate was about a factor of 10 less for gold fission than for bismuth fission. From the total cross sections obtained the average energy of neutrons detected is estimated to be between 100 and 105 Mev. Evidently the use of a higher threshold did not observably increase the ratio of  $\sigma_i/\sigma_t$  above the bismuth-fission values. Both methods of detection agree within the statistical errors.

An experiment was made to determine the angular distribution of elastically scattered neutrons from a carbon sphere. A fission chamber mounted on a radial arm pivoted below the sphere was used as the detector. The distribution is plotted in Fig. 7.

## DISCUSSION OF RESULTS

The Transparent Nucleus Model. Fernbach, Serber, and Taylor,<sup>3</sup> in a recent paper, have assumed a model for nuclei bombarded by high-energy neutrons, in which the nucleus is regarded as a sphere of material characterized by an absorption coefficient and index of refraction, both of which are functions of the neutron momentum. Using their notation,  $k_1$  is the increase of the propagation vector of the neutron wave upon entering the nucleus, and  $K$  is the absorption coefficient. A wave going a distance  $X$  in nuclear matter will have its amplitude and relative phase changed by a factor  $e^{(-\frac{1}{2}K + i k_1)X}$ . The solutions for the inelastic and elastic cross sections are, respectively

$$\sigma_i = \pi R^2 \left\{ 1 - \frac{1 - (1 + 2KR) e^{-2KR}}{2K^2 R^2} \right\}$$

$$\sigma_e = 2\pi \int_0^R \left| 1 - e^{(-K + 2i k_1)s} \right|^2 s ds$$

The form for  $\sigma_e$  is merely indicated, as the integrated expression is quite complex.  $P$  is the radius of the nucleus, and  $\sigma_t = \sigma_i + \sigma_e$ .

Taylor has determined  $k_1 = 2.85 \times 10^{12} \text{ cm}^{-1}$  and  $K = 3.0 \times 10^{12} \text{ cm}^{-1}$  to give the best straight-line fit for the radii calculated from the total cross sections when  $R$  is plotted as a function of  $A^{1/3}$ . The equation for the line of best fit is  $R = 1.38 A^{1/3} \times 10^{-13} \text{ cm}$ .

The ratio of  $\sigma_i/\sigma_t$  for the aforementioned values of  $K$  and  $k_1$  is given as a function of  $KR$  in Fig. 9, and the experimental values are shown.

Comparison with Data at 83 Mev. Cook, McMillan, Peterson, and Sewell<sup>1</sup> have measured total cross sections of the same elements in this laboratory, using carbon disks, which have a 20-Mev threshold for the  $C^{12}(n,2n)C^{11}$  reaction, for detectors. The average energy of the neutrons detected in their experiments is estimated to be 83 Mev, as compared to 95 Mev for bismuth fission. The 95-Mev cross sections are roughly 10 per cent smaller than those derived using carbon disks, indicating greater transparency at the higher energy.

## ACKNOWLEDGMENTS

The authors wish to express their gratitude to Dr. Burton J. Moyer for his help and suggestions in carrying out the program, to the cyclotron crew for their cooperation in performing the experiments, and to Dr. E. Segrè, E. Kelly, and C. Wiegand for use of their vacuum evaporator for plating the chamber disks with bismuth and gold. The work was performed under the auspices of the Atomic Energy Commission.

# APPENDIX

Effect of Path Length on Inelastic Cross-Section Measurements. If  $I_0$  is the number of neutrons per square centimeter incident on a plane absorber of thickness  $L$ , the number of neutrons per square centimeter suffering  $p$  elastic scattering events in traversing the material is given by

$$I_p L = I_0 \left( \frac{L}{\lambda_e} \right)^p \frac{1}{p!} e^{-\frac{L}{\lambda_t}} \quad (A)$$

where  $\lambda_e$  and  $\lambda_t$  are the mean free paths for elastic scattering and for any type of collision, respectively.

If  $d\sigma_e(\theta)/d\omega$  is the differential cross section per unit solid angle for elastic scattering at angle  $\theta$ , the number of neutrons per square centimeter emerging with angles between  $\theta$  and  $\theta + d\theta$  with respect to the incident neutrons is

$$dI_\theta = I_0 \sum_{p=1}^{\infty} \left( \frac{L}{\lambda_e} \right)^p \frac{1}{p!} e^{-\frac{L}{\lambda_t}} \frac{1}{p} \frac{d\sigma_e\left(\frac{\theta}{\sqrt{p}}\right)}{d\omega} \frac{2\pi \sin \theta d\theta}{\sigma_e} = I_p L \frac{1}{p} \frac{d\sigma_e\left(\frac{\theta}{\sqrt{p}}\right)}{d\omega} \frac{2\pi \sin \theta d\theta}{\sigma_e} \quad (B)$$

where it has been assumed that the effect of  $p$  elastic scatterings on the angular distribution is to broaden the distribution by a factor of  $\sqrt{p}$  and to decrease its height by  $1/p$ . Formulas A and B are only approximate, since the path length is equal to  $L$  for small angles only.

The probability of a neutron emerging at angle  $\theta$ , after sustaining an elastic collision into the  $\theta$  direction within an element  $dx$  at depth  $x$ , is

$$e^{-\frac{x}{\lambda_t}} dx \lambda_e \cdot e^{-\left(\frac{L-x}{\lambda_t \cos \theta}\right)}$$

The average attenuation experienced by neutrons following such a path is, from the above expression,

$$\frac{1}{L} \int_0^L e^{-\frac{1}{\lambda_t} \left( x + \frac{L-x}{\cos \theta} \right)} dx$$

The ratio of this attenuation at angle  $\theta$  to the attenuation when  $\theta = 0$  is the relative probability of emergence for a neutron at angle  $\theta$  compared with  $\theta = 0$ .

After integrating, the result is

$$R_A = \frac{\lambda_t}{L} \frac{\cos \theta}{1 - \cos \theta} \left[ 1 - e^{-\frac{L}{\lambda_t} \left( \frac{1}{\cos \theta} \right)^{-1}} \right]$$

The chance of a neutron inducing fission in the bismuth layer is proportional to its path length in the layer or to  $1/\cos \theta$ , since the chamber plates are normal to the undeviated neutrons.

In an elastic scattering event in the attenuator the scattered neutron will lose an amount of energy given by

$$\Delta E = \frac{2 m E (1 - \cos \theta)}{M + m (1 - \cos \theta)}$$

where  $m$  is the neutron mass,  $M$  is the mass of the nucleus, and  $E$  is the energy of the incident particle. Since the fission cross section is a function of energy, the relative chance of producing a fission is

$$\sigma_f \frac{(E - \Delta E)}{\sigma_f(E)}$$

The probability of detecting a neutron scattered through angle  $\theta$  relative to the probability of detecting an undeflected neutron is the product of the above factors

$$\frac{\pi_\theta}{\pi_0} = \frac{1 - e^{-n_t} \left( \frac{1 - \cos \theta}{\cos \theta} \right)}{n_t (1 - \cos \theta)} \sigma_f \frac{(E - \Delta E)}{\sigma_f(E)} \quad (C)$$

where  $n_t = L/\lambda_t$ , the number of total mean free paths of attenuator.

The change in the bismuth-fission cross section is given approximately by

$$\frac{d\sigma_f}{\sigma_f} = 9/4 \frac{dE}{E}$$

in the region of 90 Mev.

In our "poor geometry" experiments either  $n_t$  was small or the average angle of deviation was small (owing to forward peaking of elastically scattered particles from heavy nuclei), so the exponent in equation C may be expanded:

$$\begin{aligned} \frac{\pi_\theta}{\pi_0} &= \frac{1 - \left[ 1 - n_t \left( \frac{1 - \cos \theta}{\cos \theta} \right) + \frac{n_t^2}{2} \left( \frac{1 - \cos \theta}{\cos \theta} \right)^2 + \dots \right]}{n_t (1 - \cos \theta)} \frac{\sigma_f(E - \Delta E)}{\sigma_f(E)} \\ &\approx \left[ \frac{1}{\cos \theta} - \frac{n_t (1 - \cos \theta)}{2 \cos^2 \theta} \right] \frac{\sigma_f(E - \Delta E)}{\sigma_f(E)} \end{aligned} \quad (C)$$

If we know the angular distribution of elastically scattered neutrons, we can correct the inelastic cross section data, using  $C'$ . For carbon the relative angular distribution of scattered neutrons in the annular region between  $\theta$  and  $\theta + d\theta$  is shown in Fig. 7. If the latter curve is multiplied by  $C'$ , which has been evaluated for carbon, the area under the curve increases by about 1.2 per cent. Hence the number of singly scattered neutrons detected in the "poor geometry" experiment was increased by 1.2 per cent owing to the increased probability of detection for  $\theta > 0$ .

From A with  $(L/\lambda_e) = 0.33$  the relative number of neutrons emerging which were elastically scattered  $p$  times may be determined:

$p = 0$  : 71 per cent

$p = 1$  : 25 per cent

$p = 2$  : 4 per cent

Those scattered once and twice will have a greater probability of detection, and the increase in the total number of detector counts was roughly  $0.25 \times 1.2$  per cent +  $0.04 \times 1.5$  per cent (allowing a greater correction for double scattering), or 0.36 per cent. This increase in the detector counts caused the inelastic cross section to be low by the increase divided by the number of inelastic mean free paths,  $0.36\%/0.27$ , or about 1.3 per cent. Since the statistical error is 3.3 per cent, this correction is hardly significant.

The correction for the heavier nuclei is less, owing to the greater forward peaking of the elastically scattered neutrons.

#### REFERENCES

1. L. Cook, E. McMillan, J. Peterson, and D. Sewell, Phys. Rev., 75: 7 (1949).
2. C. Wiegand, Rev. Sci. Instruments, 19: 790 (1948).
3. S. Fernbach, R. Serber, and T. B. Taylor, Phys. Rev., 75: 1352 (1949).
4. R. Serber, Phys. Rev., 72: 1008 (1947).
5. A. C. Helmholz, E. McMillan, and D. Sewell, Phys. Rev., 72: 1003 (1947).
6. J. Hadley, E. Kelly, C. Leith, E. Segrè, C. Wiegand, and H. York, Phys. Rev., 75: 357 (1949).
7. K. Brueckner, W. Hartsough, E. Hayward, and W. Powell, Phys. Rev., 75: 555 (1949).
8. E. L. Kelly and C. Wiegand, Phys. Rev., 73: 1135 (1948).

Table 1 — Total Cross Sections for 96-Mev Neutrons Measured with Bismuth-Fission Chambers

Element	Density, g/cm <sup>3</sup>	Atomic number, Z	Mass number, A	A <sup>1/3</sup>	Cross section $\sigma_t \times 10^{24}$ cm <sup>2</sup>	Radius, R $\times 10^{13}$ cm from model
Hydrogen		1	1	1.00	0.0745 $\pm$ .002 0.073 $\pm$ .003 0.071 $\pm$ .002 0.073 $\pm$ .0015	1.69 .02
Deuterium		1	2	1.26	0.104 $\pm$ .004	1.89 .03
Beryllium	1.847	4	9	2.08	0.396 $\pm$ .004	2.94 .015
Carbon	1.580	6	12	2.29	0.502 $\pm$ .004 0.502 $\pm$ .005 0.490 $\pm$ .004 0.494 $\pm$ .004 0.501 $\pm$ .006 0.498 $\pm$ .003	3.20 .01
Nitrogen		7	14	2.41	0.570 $\pm$ .007	3.35 .02
Oxygen		8	16	2.52	0.663 $\pm$ .007	3.52 .02
Aluminum	2.714	13	27	3.00	0.993 $\pm$ .011	4.11 .02
Chlorine		17	35.46	3.29	1.28 $\pm$ .02	4.55 .03
Copper	8.90	29	63.57	3.99	2.00 $\pm$ .02 2.00 $\pm$ .03	5.53 .03
Tin	7.28	50	118.7	4.92	3.18 $\pm$ .03 (3.13)*	6.81 .03
Lead	11.33	82	207.2	5.92	4.48 $\pm$ .03 (4.38)	8.14 .03
Uranium	18.89	92	238.1	6.20	4.92 $\pm$ .06 (4.89)	8.58 .05
Deuterium- Hydrogen		0	1	1.00	0.031 $\pm$ .002	
Compounds						
H <sub>2</sub> O	0.998				0.815 $\pm$ .005 0.807 $\pm$ .005	
D <sub>2</sub> O	1.104				0.868 $\pm$ .005	
Pentane	0.627				3.40 $\pm$ .03	
C <sub>5</sub> H <sub>12</sub>					3.37 $\pm$ .03 3.32 $\pm$ .02	
CCl <sub>4</sub>	1.592				5.61 $\pm$ .07	
Melamine C <sub>3</sub> H <sub>6</sub> N <sub>6</sub>					5.37 $\pm$ .035	

\*Values in parentheses are not corrected for diffraction scattering.

Table 2

Element	$\frac{\sigma_i}{\sigma_t}$	$\sigma_t \times 10^{24} \text{ cm}^2$	Total M. F. P. used
Carbon	$0.460 \pm .016$	$0.496 \pm .012$	0.60
	$0.457 \pm .026$	$0.489 \pm .018$	
	$0.434 \pm .023$	$0.497 \pm .017$	
	$0.431 \pm .024$	$0.498 \pm .017$	
	$0.454 \pm .022$	$0.502 \pm .016$	
Aluminum	$0.42 \pm .015$	$0.995 \pm .02$	0.94 (dural)
Copper	$0.39 \pm .005$	$2.005 \pm .02$	2.5
Lead	$0.40 \pm .01$	$4.46 \pm .06$	1.9
	$0.38 \pm .01$	$4.46 \pm .06$	
	$0.40 \pm .01$		
Carbon (ave.)	$0.45 \pm .015$	$0.497 \pm .008$	

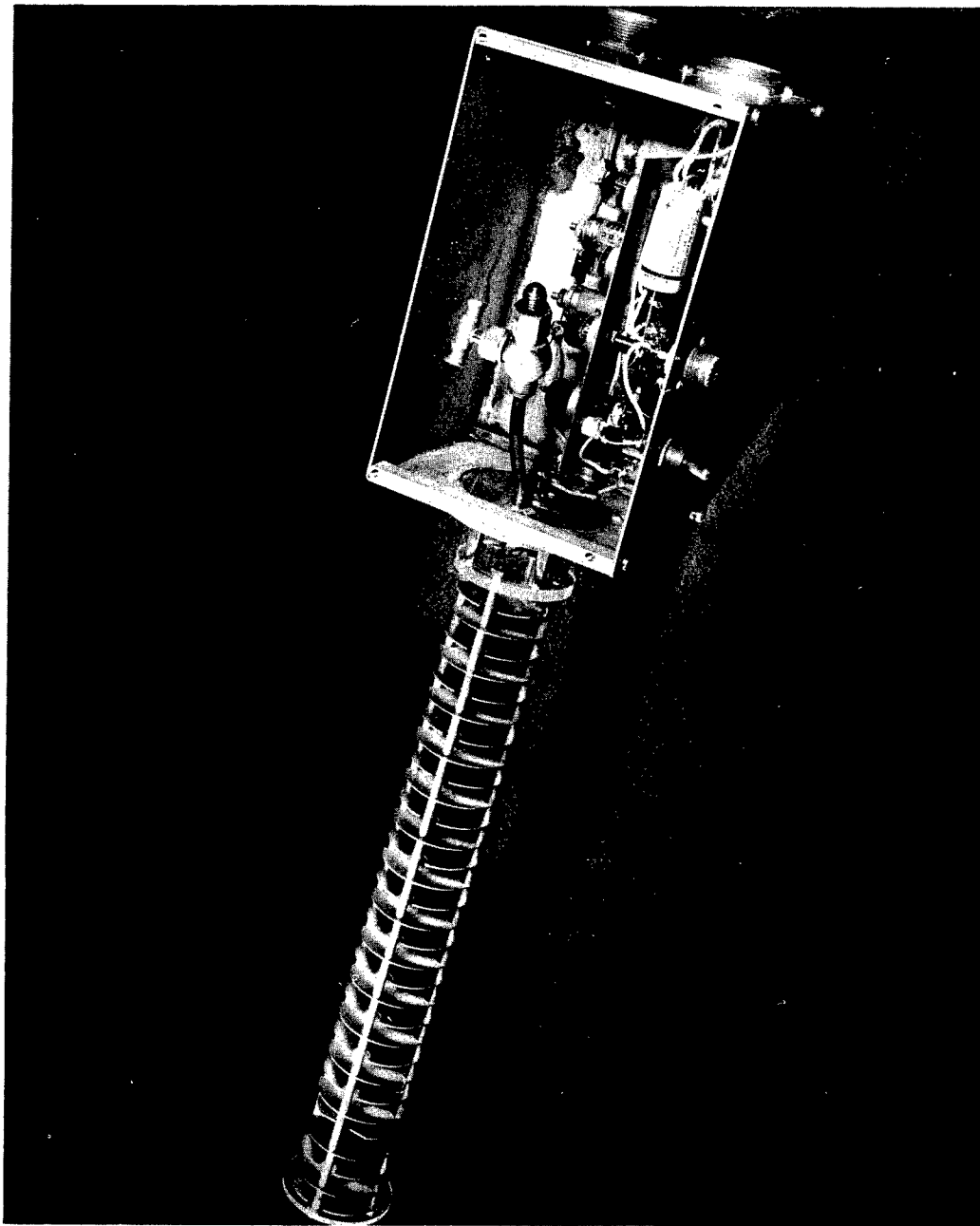


Fig. 1 — Internal structure of long-fission ionization chamber.

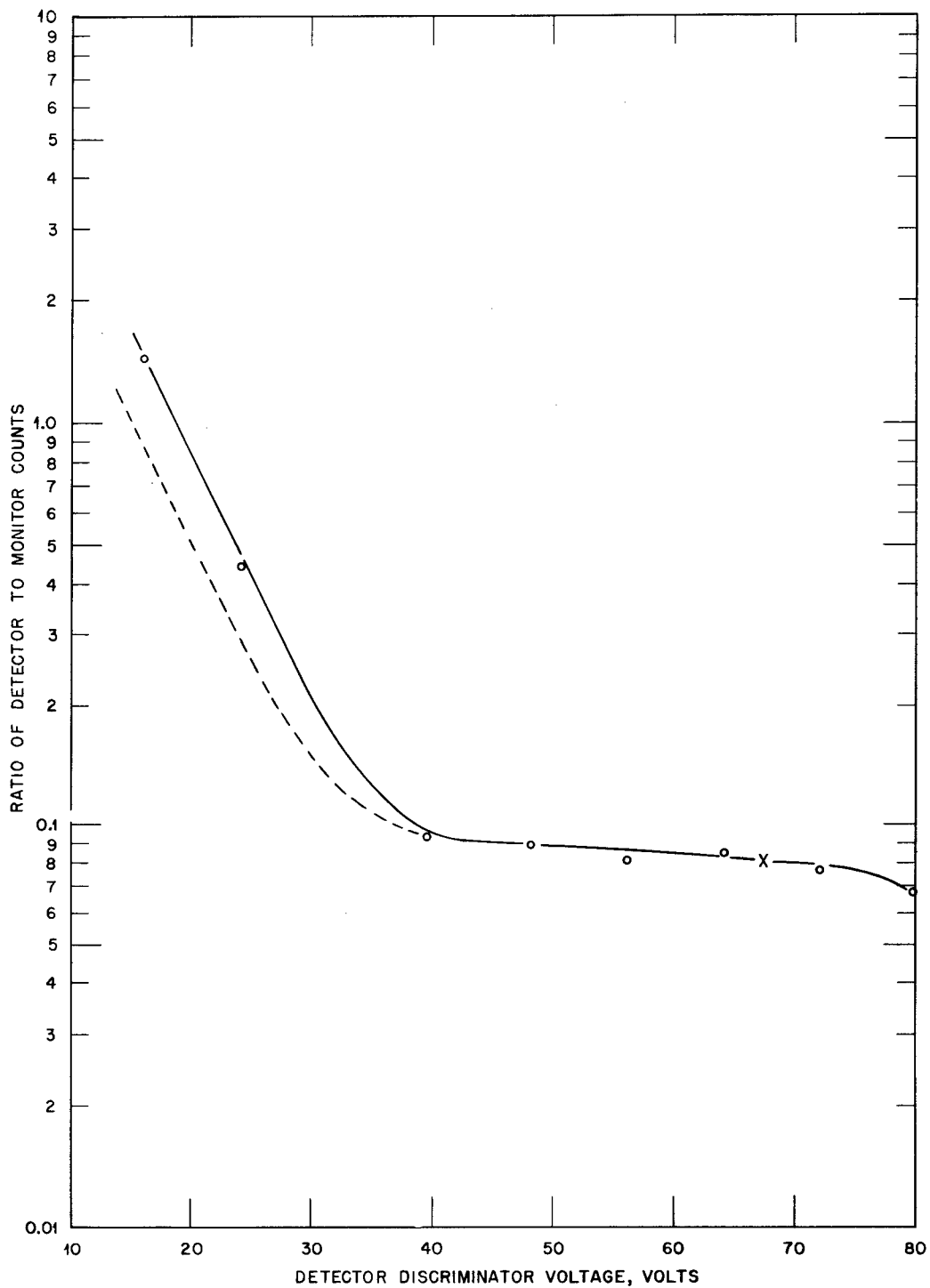


Fig. 2—Discriminator curve; number of pluses greater than disk voltage vs. disk voltage. Dotted curve is at neutron intensity half that of solid curve. X, operating point.

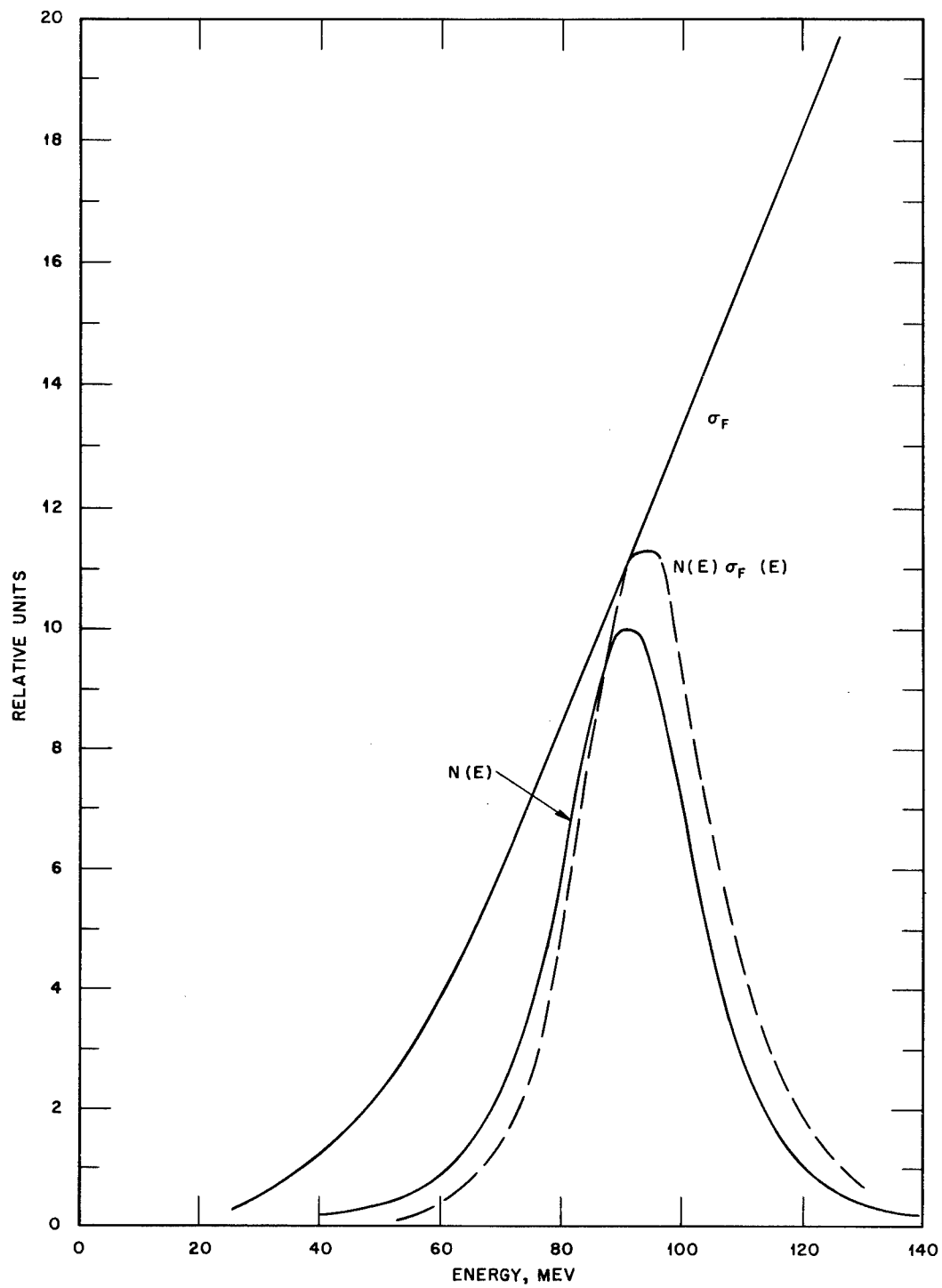


Fig. 3— $\sigma_F$ , fission cross section of bismuth;  $N(E)$ , energy distribution of neutrons;  $N(E) \sigma_F(E)$ , detection efficiency.

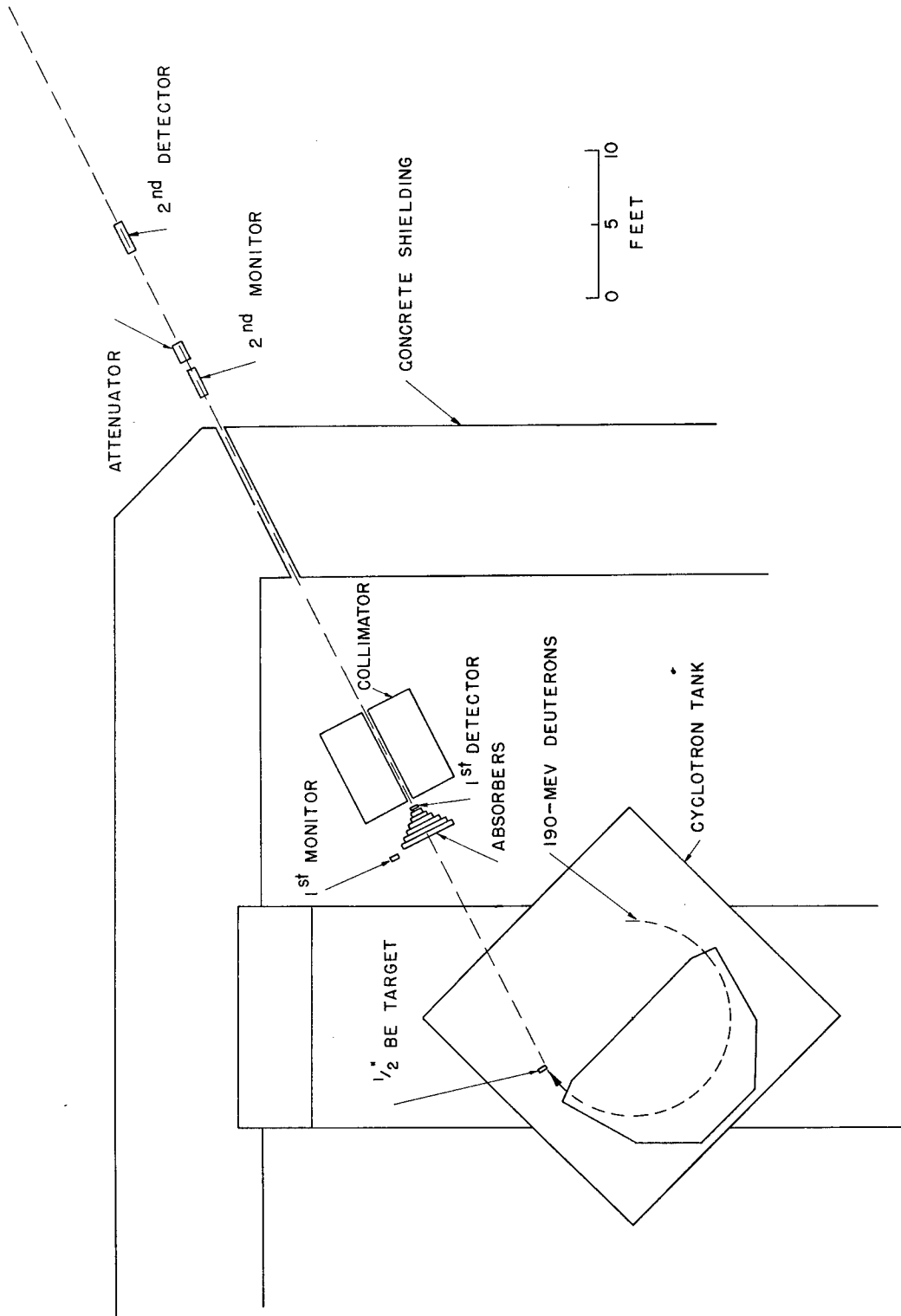


Fig. 4—Arrangement of apparatus.

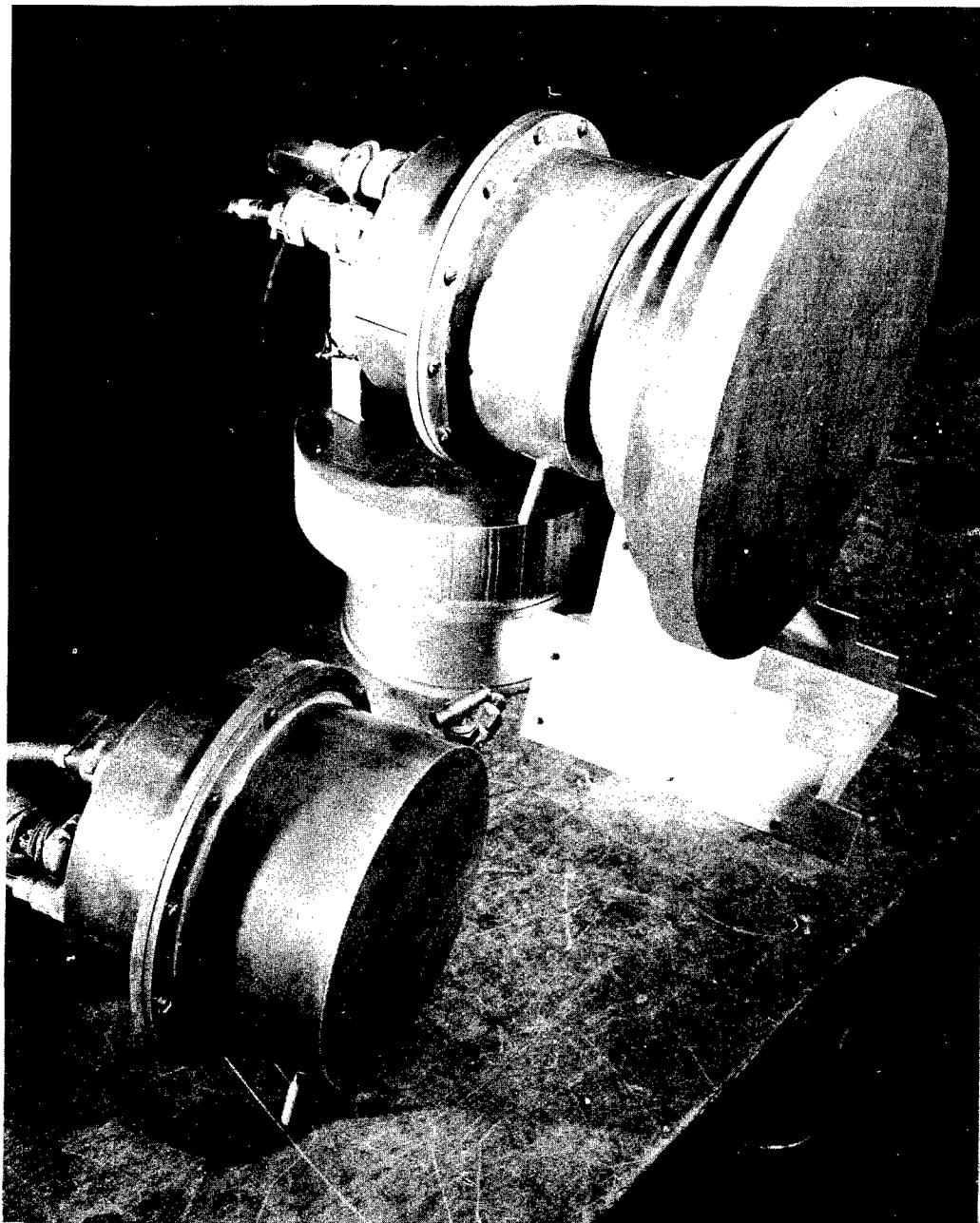


Fig. 5—Fission chambers and absorbers used in "poor geometry" measurements.

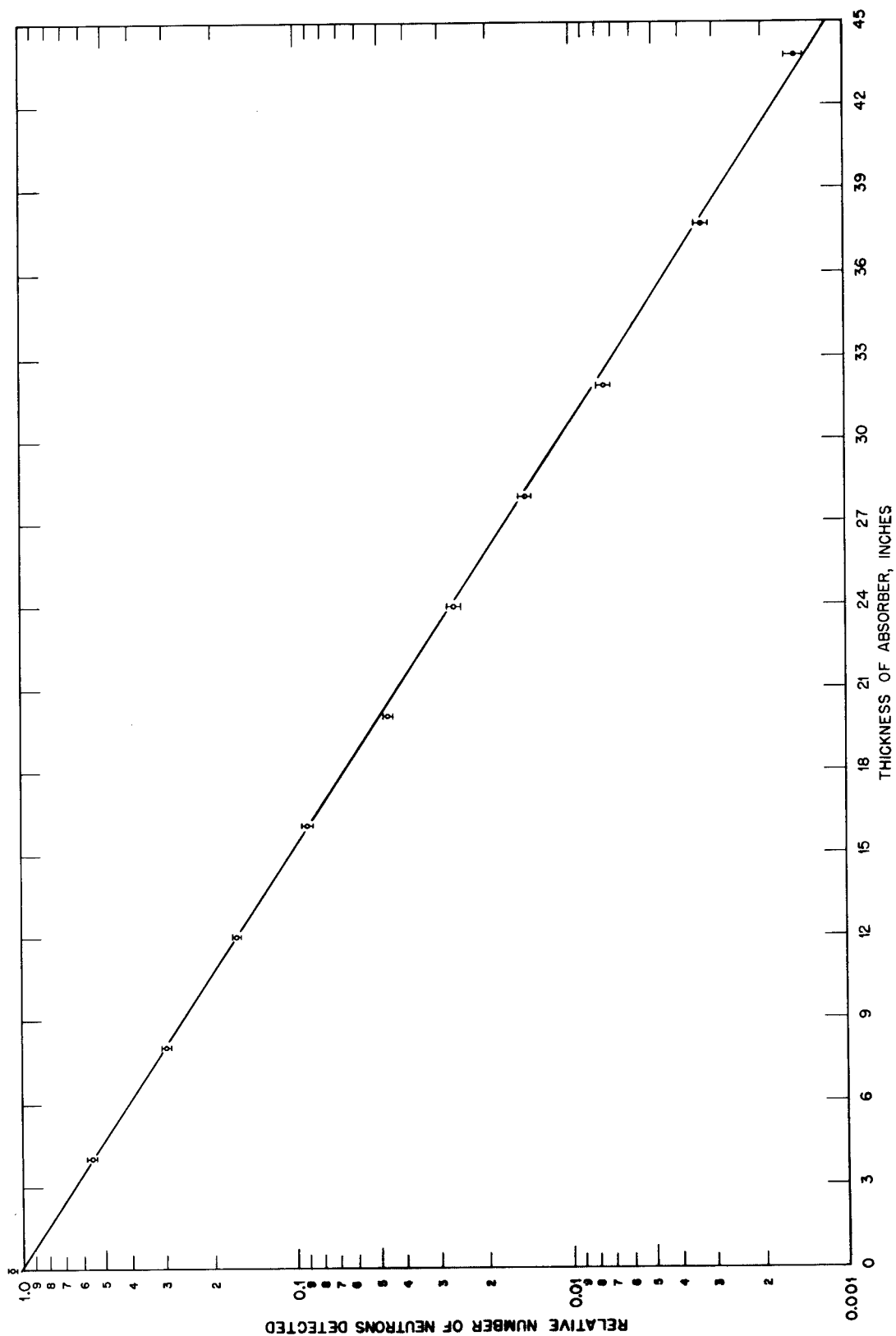


Fig. 6—Absorption of neutrons in Al.

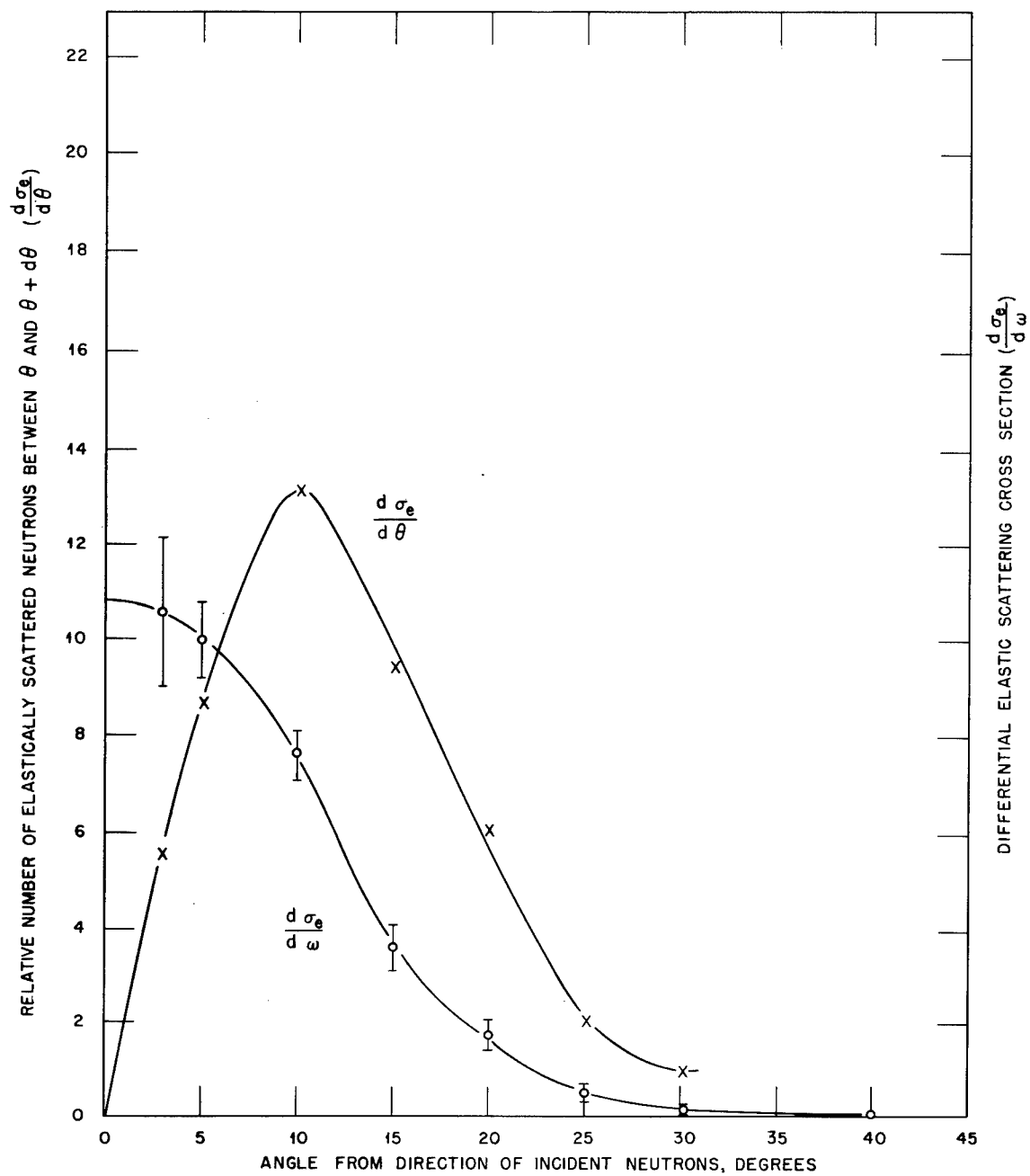


Fig. 7—Angular distribution of elastically scattered neutrons from carbon.

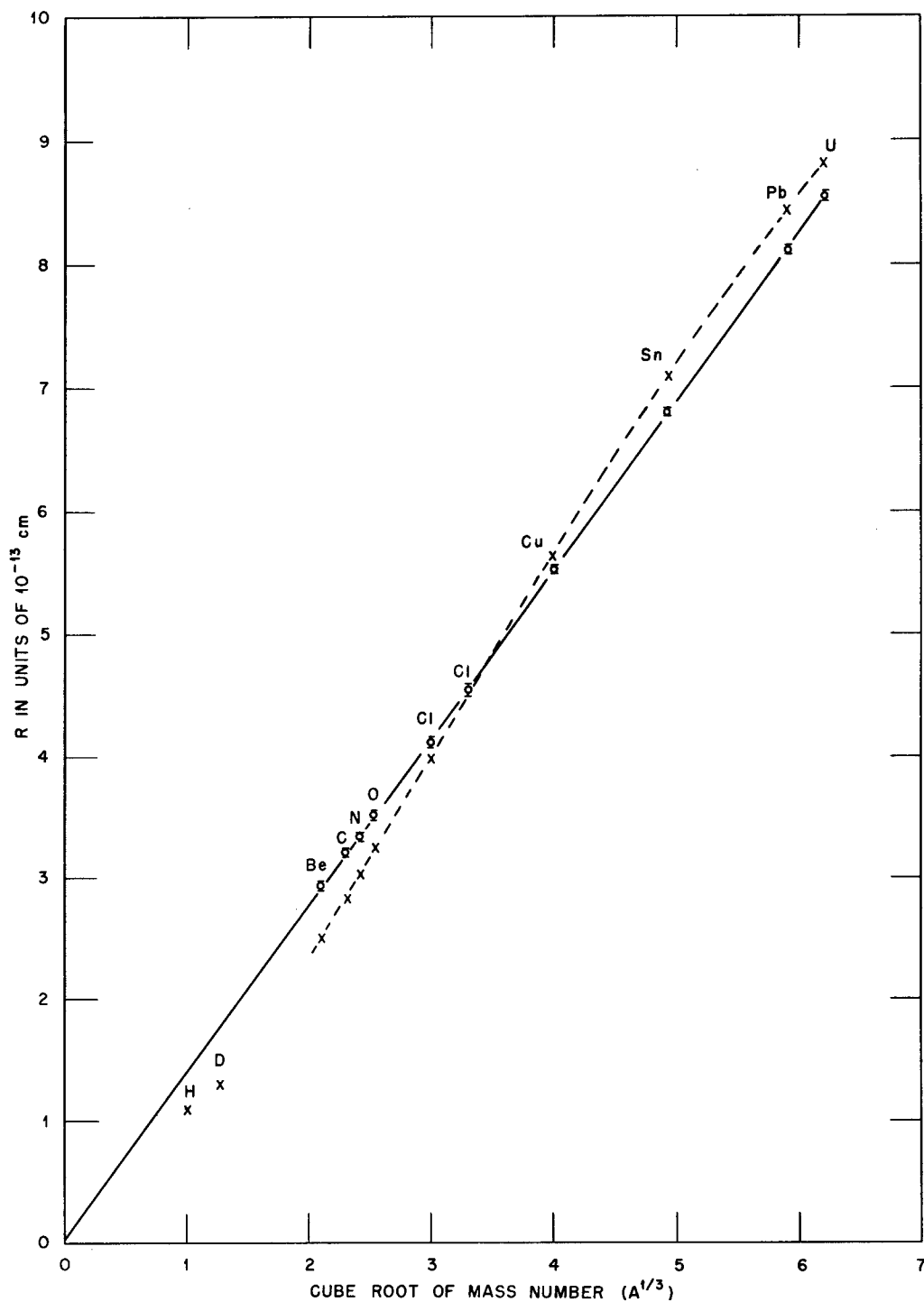


Fig. 8—Radii calculated from model assuming  $K = 3.00 \times 10^{12} \text{ cm}^{-1}$  and  $k_1 = 2.85 \times 10^{12} \text{ cm}^{-1}$  define straight line of equation  $R = 1.38 \times A^{1/3} \times 10^{-13} \text{ cm}$ . Dotted line is graph of radii calculated from  $\sigma_t = 2\pi R^2$  (opaque nucleus).

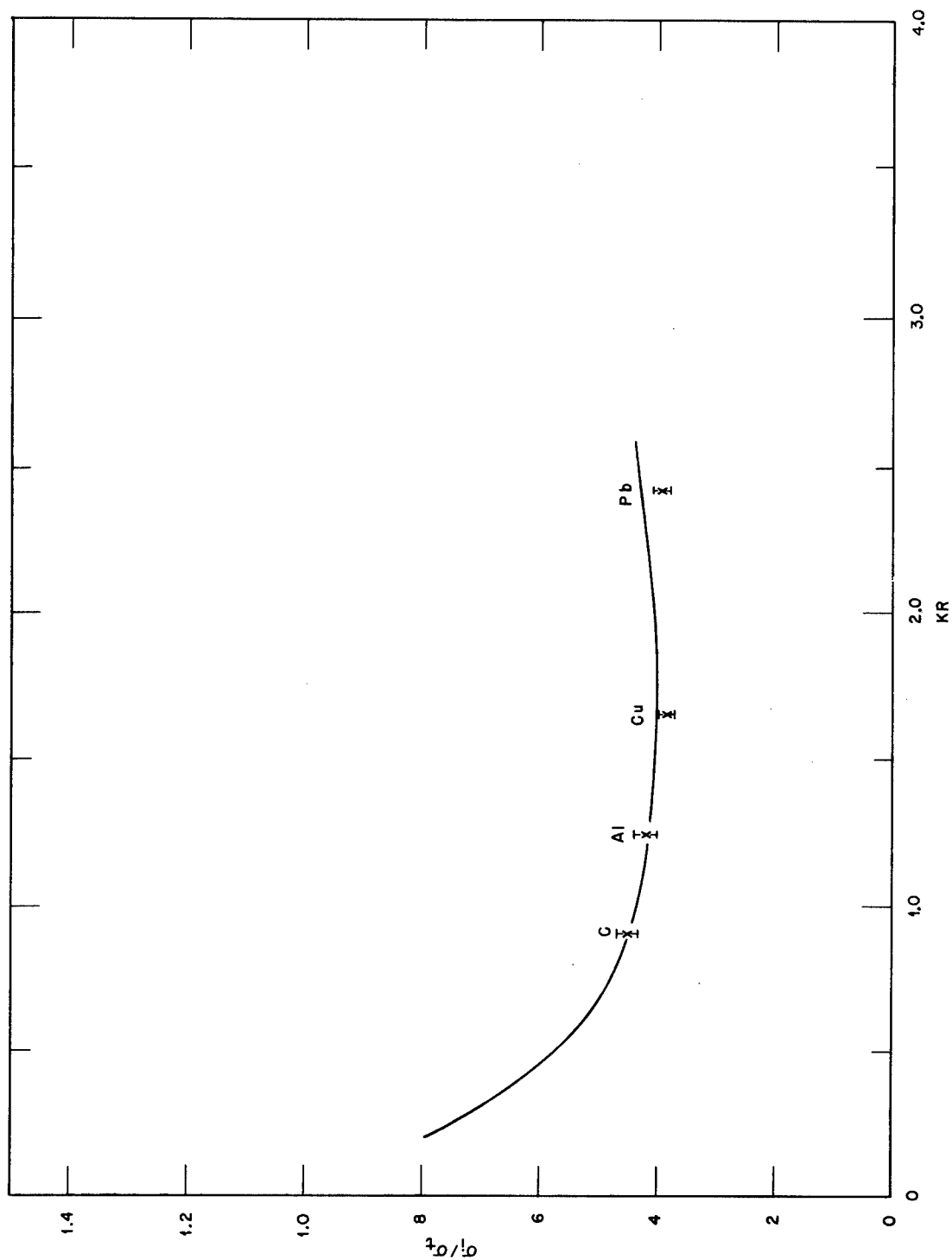


Fig. 9—Theoretical curve of  $\sigma_i/\sigma_t$  for  $K = 3.00 \times 10^{12} \text{ cm}^{-1}$  and  $k_1 = 2.85 \times 10^{12} \text{ cm}^{-1}$  with experimental points.

END OF DOCUMENT